Direct visualization of damage cascades in lithium niobate crystals caused by high-energy ions

2009 J. Phys.: Condens. Matter 21 075402

(http://iopscience.iop.org/0953-8984/21/7/075402)

J. Phys.: Condens. Matter **21** (2009) 075402 (5pp) doi:10.1088/0953-8984/21/7/075402

Direct visualization of damage cascades in lithium niobate crystals caused by high-energy ions

M R Zamani-Meymian[1], K Peithmann[1], K Maier[1], H Schmid[2] and W Mader[2]

[1] Helmholtz-Institut für Strahlen- und Kernphysik, Universität Bonn, Nussallee 14-16, D-53115 Bonn, Germany
[2] Institut für Anorganische Chemie, Universität Bonn, Römerstraße 164, D-53117 Bonn, Germany

Received 20 November 2008
Published 29 January 2009
Online at stacks.iop.org/JPhysCM/21/075402

Abstract
Congruently melting undoped lithium niobate crystals are irradiated with 20 MeV ^{3}He ions which penetrate the entire crystal volume. Radiation damage effects are directly visualized by transmission electron microscopy (TEM) where damage zones with diameters of 4 nm give rise to circular Fresnel fringe contrasts. These regions of modified material, appearing circular in cross-section, are interpreted as damage cascades inflicted by fast Nb and O atoms displaced in knock-on collisions with primary ^{3}He ions. This two-step displacement process results in local density changes manifested by the contrast behaviour of Fresnel fringes observed in TEM images.

1. Introduction

Lithium niobate crystals ($LiNbO_3$) play a substantial role in nonlinear optical materials applications for holographic data storage [1, 2], wavelength division multiplexers (WDM) for optical communication networks [3, 4], and integrated optics in components like integrated lasers [5] and modulators [6]. The latter are based on the feasibility of preparing waveguides in $LiNbO_3$ by various methods. Commonly used methods are (i) indiffusion of Ti into a near-surface volume of the crystal, forming a waveguiding layer or channel [7, 8], and (ii) exchange of protons [9]. Alternatively, waveguides can be fabricated by implantation of low-mass ions like helium [9–12]. High-energy ions (e.g. He ions) entering the crystal are stopped at a certain penetration depth within some 10 μm where the material structure is strongly damaged within a buried layer with thickness given by the straggling range. The refractive index of this stopping layer thus changes in comparison to undamaged crystal regions. Light can now be guided between the surface and the stop layer. Additionally, in the waveguiding layer itself the refractive index of the crystal is changed too: an increase of the extraordinary index Δn_e has been reported [11]; even amorphization of certain layers of material has been found when ions like F are employed [13]. Besides these methods of waveguide fabrication close to the crystal surface, irradiating $LiNbO_3$ with low-mass, high-energy ions like ^{3}He at 41 MeV changes the refractive index of the material over the whole volume penetrated by the ions, which extends to the stopping depth of the ions exceeding 0.5 mm. This approach yields large Δn of the order of 5×10^{-3} [14, 15] and can be used to structure embedded waveguides [16]. It is of advantage that these waveguides are embedded and that the waveguiding material itself consists of non-irradiated material with unchanged material parameters.

When the fast ions interact with the crystal, distinct modifications of the material occur. However, the details of the mechanisms causing the refractive index to change are unknown. Commonly the magnitude of the changes is linked to the differential energy loss $\Delta E/\Delta x$ (stopping power) of the ions in a certain material depth. In the case of ^{3}He irradiation, however, a recent study indicates a direct correlation of the total concentration of vacancies c_{vac}, representing atomic displacements calculated using SRIM2003 [17], produced by the projectile in the crystal. Theoretical approaches assume small clusters of amorphous material embedded within a crystalline structure. In this contribution we present transmission electron microscopic (TEM) measurements performed on irradiated material revealing a direct visualization of damages induced by high-energy ^{3}He ions.

2. Experimental methods

Commercially available lithium niobate crystals ($LiNbO_3$) with congruently melting composition are cut from undoped wafer material in z-cut geometry. To obtain TEM samples in plan view, standard techniques (cutting, grinding, dimpling, and Ar sputtering) are applied. Irradiation of the dimpled sample with high-energy ions is carried out on a cyclotron (Helmholtz Institute, University of Bonn). ^{3}He ions accelerated to an energy of 40 MeV are focused into a beam with a diameter of 5 mm and total ion current of 20 nA. The previously dimpled sample is irradiated for 11 h, corresponding to a total ion dose of 1.3×10^{20} ions m^{-2}. To increase the interaction of the ions with the $LiNbO_3$ target, the ion energy is attenuated by passing the beam through an aluminium foil with a thickness of 540 μm; hence the ion energy is diminished to ≈20 MeV without notably changing the other beam parameters. The ion range of ^{3}He ions in $LiNbO_3$ is approximately 160 μm for an energy of ≈20 MeV and thus exceeds the sample thickness of 40 μm. According to SRIM calculations, 99.995% of the ^{3}He ions are transmitted through the entire crystal; hence implantation of ^{3}He can be neglected. The crystals are placed outside the beamline vacuum beyond a thin aluminium window (thickness 30 μm). To check whether the irradiation process induces changes in the material, a graphite aperture is placed in front of the sample to shade half of the crystal; hence irradiated and non-irradiated material is present in the same sample.

Irradiated samples are thinned by Ar sputtering and are investigated in a TEM operated at 300 kV (Philips CM300UT FEG TEM/STEM). Images are recorded on a 2k CCD camera; the achievable structural resolution is ≈0.2 nm.

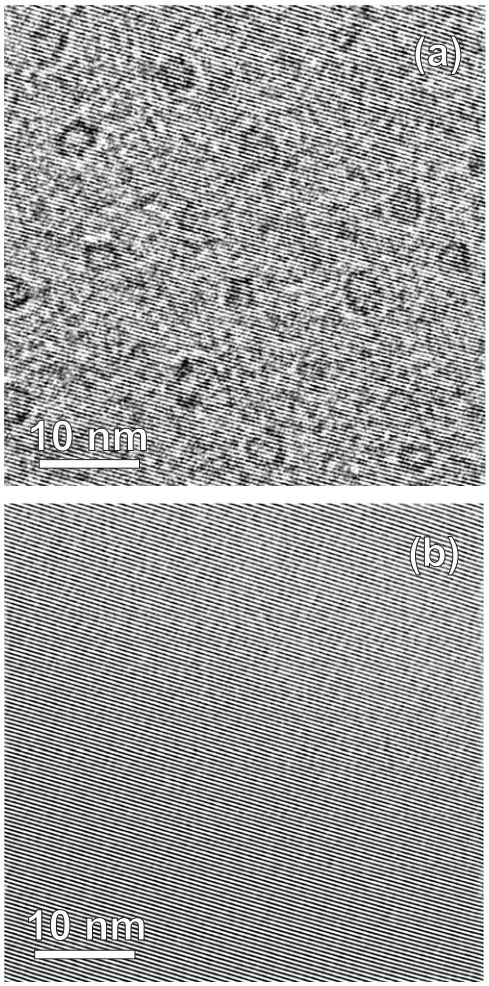

Figure 1. TEM lattice fringe images of $LiNbO_3$ crystal: (a) ^{3}He ion irradiated crystal region showing circular damage features; (b) non-irradiated crystal part shown for comparison.

3. Results and discussion

A medium-thick section (thickness ≈20 nm) of the irradiated part of the crystal is shown in figure 1(a); a section of the non-exposed crystal part is shown as image (b) for comparison. Both images are taken in [$\bar{2}$110] zone axis (ZA) orientation, i.e. with the incident electron beam parallel to the [$\bar{2}$110] direction, and clearly show the ($0\bar{1}1\bar{2}$) type lattice fringes of the $LiNbO_3$ matrix structure (lateral spacing $d_{0\bar{1}1\bar{2}} = 0.375$ nm).

Beside the lattice fringes, also distinct circular features ≈3–5 nm in diameter, which are not detected in the non-exposed crystal part, are clearly visible in images from irradiated sample regions. The grainy background contrasts visible in the TEM images are essentially due to an amorphization in the surface layers (thickness: ≈2 nm) as a result of Ar ion sputtering. Due to the absence of circular features in figure 1(b) we can be sure that the Ar sputtering process does not contribute to the irradiation effect under investigation. However, as a consequence of the Ar sputtering, an ≈10 nm wide rim of structurally disordered material extends along the edge of the wedge shaped sample (see figure 2(a)). It is noted that, besides the surface damage, contrasts appear blurred in images from irradiated sample parts due to structural damage of the bulk. Both lattice fringes and circular features are best visible in medium-thick specimen regions with 5–25 nm thickness; these contrasts are increasingly blurred by amplitude contrasts (absorption) in thicker crystal parts. The framed area in figure 2(a) is shown in more detail in figure 2(b). Both ($0\bar{1}1\bar{2}$) and ($0\bar{1}14$) lattice fringes are imaged (ZA [$\bar{2}$110]). Although lattice fringes continue across the circular features, contrast within is blurred and fringes are distorted and/or displaced. In regions between circular features only small patches of crystalline matrix appear to remain undisturbed by the ^{3}He ion irradiation.

The contrast behaviour of circular features is studied in TEM bright-field (BF) imaging mode; the results are shown in figure 3. It is well known that any discontinuity, such as the edge of the sample or internal interphase interfaces, gives rise to Fresnel fringe contrasts under out-of-focus imaging conditions due to variation of the inner potentials [18]. At the specimen–vacuum interface the sequence of dark and bright contrast fringes is terminated by a bright fringe facing the vacuum (lower potential) in under-focus conditions (see figure 3(a)); in over-focus conditions an inverted fringe sequence is observed (figure 3(b)). Interfaces between the circular features (e.g. the one indicated by the dotted circle) and their surrounding matrix exhibit an analogous contrast

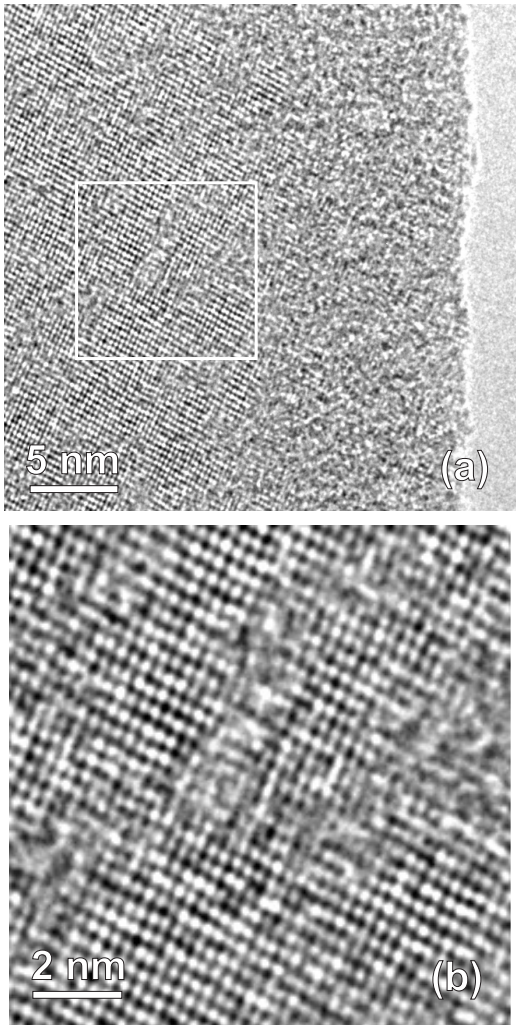

Figure 2. TEM image showing a region close to the edge of the Ar milled hole in the sample. (a) Circular damage features are visible in the medium-thick crystal region; an ≈10 nm wide zone of Ar ion damaged material is observed along the specimen edge. Part (b) shows the framed area of (a) in more detail: although the $(0\bar{1}1\bar{2})$ and $(0\bar{1}14)$ lattice fringes continue across the circular features, fringes are distorted and/or displaced, and the contrast is blurred (ZA $[\bar{2}110]$).

behaviour (figures 3(a), (b), bottom), i.e. terminated by bright or dark fringes in under- and over-focus cases, respectively. This contrast behaviour, indicative of a discontinuity in the inner potential, is consistent with the assumption of an increased material density within the circular features induced by ^{3}He irradiation in comparison with the surrounding undisturbed matrix.

As pointed out above, the interaction of ^{3}He ions with $LiNbO_3$ causes local density enhancements within the crystal volumes traversed by high-energy ions. To explain the size and nature of the changes we assume that initially a fast ^{3}He ion in a knock-on process hits one Nb atom in the crystal and passes a part of its energy to it: a central collision yields a maximum energy transfer of ≈2.4 MeV onto the Nb atom which by far exceeds the threshold energy for atom displacement, as illustrated schematically in figure 4. Simulations using SRIM-2003 for this high-energy Nb ion yield a range of 0.8 μm in $LiNbO_3$ with a lateral straggling range of 0.15 μm, as indicated in figure 4. On its trajectory, the Nb ion loses its entire energy at a rate of ≈3 keV nm^{-1}. Displacement cascades are created along the stopping path, resulting in a cylindrical volume of modified material traversed by the Nb ion. Besides Nb, two other ions can be at play: O and Li. A knock-on collision of ^{3}He with an O ion yields a maximum energy transfer of 10 MeV, exhibiting a trajectory of 4 μm. This determines an energy loss of 2.5 keV nm^{-1}. Finally, an energy of 17 MeV could be transferred to a Li atom; however, due to their low mass, such atoms have a trajectory of 30 μm yielding an energy loss of 0.5 keV nm^{-1}. SRIM simulations yield that knock-on collisions of ^{3}He ions with O are twice as probable as collisions with Nb; hence both processes are reasonable and have to be considered.

After ^{3}He irradiation, electron transparent foils for TEM investigations are prepared by Ar milling from both sides (figure 4). Thus, only a ≈20 nm thin central section of the irradiated crystal remains accessible to TEM imaging. Hence, just a small section of the initially present damage path will be contained within the TEM sample. Since the directions of fast Nb or O atoms displaced by central collisions are strongly forward peaked, damage tracks are approximately parallel to the normal direction of the TEM foil. Thus, the cylindrical damage zones are imaged as circular features in cross-section. Diameters of observed circular features are between 3 and 6 nm, and agree well with literature reports on the sizes of damage tracks induced by ion irradiation in amorphizable insulators [19].

The formation of continuous amorphous tracks in $LiNbO_3$ crystals by the irradiation with heavy ions of threshold stopping powers between 1 and 10 keV nm^{-1} has been reported [20, 21]. Electronic excitation can be assumed as the predominant interaction mechanism for incident ions with stopping power exceeding a critical threshold value. In the thermal spike model it is assumed that within the stopping range a cylindrical volume of target material is amorphized along the ion track. In insulators with stopping power in the range of 1–5 keV nm^{-1} the apparent dependence of the track diameter on the stopping power could be explicable using this model [22, 23]. In the case of 2.4 MeV Nb ions a range of 800 nm yields a stopping power of ≈3 keV nm^{-1} in $LiNbO_3$, which lies within the range of continuous track formation [21]. Alternatively, the O ions with similar energy loss lead to the same effect. Thus, it is reasonable to attribute the circular features to damage tracks caused by Nb and O ions because their energy loss is large enough to damage the crystal structure within a cylindrical volume. Possible alternative mechanisms can be ruled out for the damage observed in $LiNbO_3$: the primary ^{3}He ions as well as Li ions displaced by central knock-on collisions exhibit much smaller specific energy losses insufficient to cause amorphization of the $LiNbO_3$. Hence the observed damage effects are attributed to a two-step mechanism via $^3\text{He} \rightarrow \text{Nb}$ and $^3\text{He} \rightarrow \text{O}$ knock-on collisions.

The area density of damage tracks is estimated from the total ion flux density of 130 ^{3}He ions nm^{-2} on the target entrance surface. Thus, a surface area of 50 × 50 nm^2 (equal to the size of specimen area imaged in figure 1) is traversed by

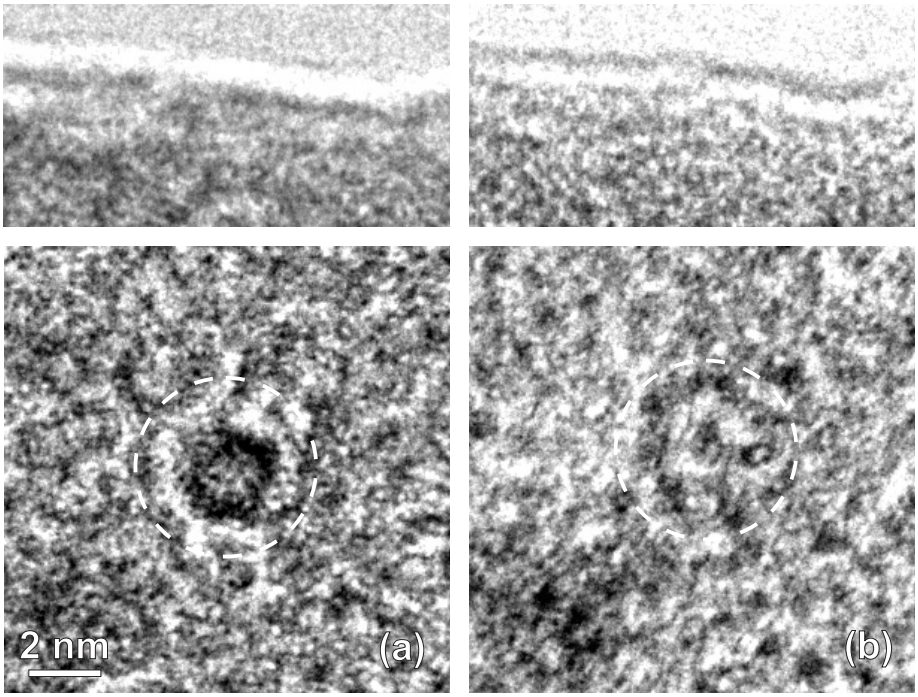

Figure 3. TEM images of the edge of the sample (upper parts) and of one circular feature induced by ^{3}He ion irradiation (lower parts). The images (a) show the crystal in under-focus mode whereas the images (b) have been taken in over-focus mode, showing the same crystal regions. At the sample edge and within the circular feature, increasing potential yields changes from white to black in the under-focus mode (part (a)) whereas the order is inverted in the over-focus mode (from black to white, part (b)).

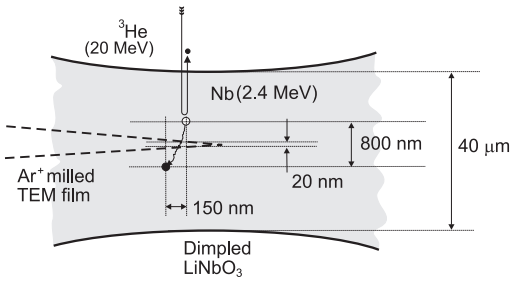

Figure 4. Schematic diagram of dimpled sample geometry and fast ion trajectories after central ^{3}He → Nb knock-on collision: the specimen region remaining after Ar sputtering is indicated by dashed lines; only short sections of Nb trajectories remain within wedge shaped TEM foil.

$n_{\mathrm{He}} = 3.3 \times 10^5$ ^{3}He ions. For collisions between 20 MeV ^{3}He ions and Nb target atoms, SRIM calculations yield a total probability of 2×10^{-4} nm^{-1} of penetration depth. Thus, within a crystal slab of 5 μm thickness each ^{3}He ion encountered on average one collision with a Nb atom. Calculating the number of collisions in the area investigated with a sample thickness of 20 nm we obtain a total of 1300 displacements. This number gives an upper limit of traceable damage tracks traversing the sample volume imaged in TEM. This has to be compared to our experiments where at least 30 circular features are detected within the specimen region imaged in figure 1. At first glance the numbers do not match in a convincing manner. However, it has to be taken into account that in just a small fraction of incidences sufficient energy is transferred in central collisions in order to form damage tracks. The majority of collision events will yield much smaller energy transfers below the threshold energy of amorphization.

It has been reported that changes of the refractive index Δn are directly correlated with the number of vacancies c_{vac} produced by the ^{3}He ions in the target material, whereas a direct link to the energy-loss function $\Delta E/\Delta x$ appears less likely [15]. This is explicable under the assumption that the observed radiation damage effects are created indirectly by high-energy Nb and O ions and not primarily by the ^{3}He ions. The number of vacancies c_{vac} is directly linked to the number of fast secondary Nb and O ions displaced by knock-on collisions with ^{3}He ions.

In summary, we propose the following explanation for the effects: the crystal damages are essentially caused by fast Nb and O atoms displaced by knock-on collisions with ^{3}He ions. Alternatively, knock-on processes via ^{3}He → Li → Nb, or ^{3}He → Li → O are also possible but at lower probability. The fast Nb and O ions lose their energy by electronic excitation within a cylindrically shaped crystal volume according to the thermal spike model. Their energy loss of ≈3 keV nm^{-1} along the decelerating path is sufficient to melt or partially amorphize the material which subsequently may relax and partially recrystallize in a different phase. It is assumed that Li as the most volatile species in this ternary compound is partially removed from the damaged volume. Thus, a Li-deficient phase, e.g. $LiNb_3O_8$, is expected with similar refractive indices to $LiNbO_3$ but enhanced mass density (≈5 g cm^{-3}) [24]. This picture of a Li-deficient phase is compatible with the observed contrast behaviour of Fresnel

fringes around the circular damage zones, which indicates an increased inner potential in comparison with the surrounding matrix crystal. Li atoms can easily be accommodated in the $LiNbO_3$ crystal lattice because of an intrinsic Li deficit in the congruently melting crystal composition.

4. Conclusion

Ion irradiation is widely used for tailoring optical and ferroelectric properties of crystals like lithium niobate. Transmission electron microscopy (TEM) reveals the formation of distinct clusters of modified material as a result of irradiation with low-mass ^{3}He ions at 20 MeV. Circularly shaped features observed in cross-section are interpreted as damage tracks inflicted by Nb and O ions displaced in a two-step knock-on process. Since the contrast behaviour of Fresnel fringes indicates an enhanced material density within the damaged zones, it is concluded that Li as the most volatile species may be exuded from the cylindrically shaped damage volumes, resulting in a localized modification of Li-deficient material responsible for changes of the refractive index. Further TEM investigations, including other irradiation experiments using other ion species beside ^{3}He (e.g. swift heavy ions), appear promising for studying the mechanisms responsible e.g. for changes of the refractive index or estimating their long-term stability.

Acknowledgments

The technical support of the cyclotron team of the Helmholtz-Institut, Universität Bonn, is highly appreciated. We thank G Schröder for preparing the TEM samples. Financial support from the Deutsche Forschungsgemeinschaft (grant FOR 557 B1) is gratefully acknowledged.

References

[1] Coufal H J, Psaltis D and Sincerbox G T 2000 *Holographic Data Storage* (Berlin: Springer)
[2] Shelby R M, Hoffnagle J A, Burr G W, Jefferson C M, Bernal M-P, Coufal H, Grygier R K, Guenther H, Macfarlane R M and Sincerbox G T 1997 *Opt. Lett.* **22** 1509–11
[3] Leyva V, Rakuljic G A and O'Conner B 1994 *Appl. Phys. Lett.* **65** 1079–81
[4] Breer S, Vogt H, Nee I and Buse K 1999 *Electron. Lett.* **34** 2419–21
[5] Becker C, Greiner A, Oesselke T, Pape A, Sohler W and Suche H 1998 *Opt. Lett.* **23** 1194–6
[6] Ramaswamy V, Divino M D and Standley R D 1978 *Appl. Phys. Lett.* **32** 644–6
[7] Alferness R C, Schmidt R V and Turner E H 1979 *Appl. Opt.* **18** 4012–6
[8] Schmidt R V and Kaminow I P 1974 *Appl. Phys. Lett.* **25** 458–60
[9] Kip D 1998 *Appl. Phys.* B **67** 131–50
[10] Destefanis G L, Townsend P D and Galliard J P 1978 *Appl. Phys. Lett.* **32** 293–4
[11] Hu H, Chen F, Shi B-R, Wang K-M and Shen D-Y 2001 *Appl. Opt.* **40** 3759–61
[12] Chandler P J and Townsend P D 1987 *Nucl. Instrum. Methods Phys. Res.* B **19/20** 921–6
[13] Olivares J, Garcia G, Garcia-Navarro A, Agullo-Lopez F, Caballero O and Garcia-Cabanes A 2005 *Appl. Phys. Lett.* **86** 183501
[14] Andreas B, Peithmann K, Buse K and Maier K 2004 *Appl. Phys. Lett.* **84** 3813–5
[15] Peithmann K, Zamani-Meymian M-R, Haaks M, Maier K, Andreas B and Breunig I 2006 *J. Opt. Soc. Am.* B **23** 2107–12
[16] Peithmann K, Zamani-Meymian M-R, Haaks M, Maier K, Andreas B, Buse K and Modrow H 2006 *Appl. Phys.* B **82** 419–22
[17] Ziegler J F, Biersack J P and Littmark U 1985 *The Stopping and Range of Ions in Solids* (New York: Pergamon)
[18] Schmid H K 1999 *J. Microsc.* **194** 192–202
[19] Toulemonde M, Dufour C, Meftah A and Paumier E 2000 *Nucl. Instrum. Methods Phys. Res.* B **166/167** 903–12
[20] Canut B, Brenier R, Meftah A, Moretti P, Salem S O, Ramos S, Thevenard P and Toulemonde M 1994 *Nucl. Instrum. Methods Phys. Res.* B **91** 312–6
[21] Itoh N and Stoneham A M 1998 *Nucl. Instrum. Methods Phys. Res.* B **146** 362–6
[22] Meftah A, Brisard F, Costantini J M, Hage-Ali M, Stoquert J P, Studer F and Toulemonde M 1993 *Phys. Rev.* B **48** 920–5
[23] Szenes G 2002 *Nucl. Instrum. Methods Phys. Res.* B **191** 54–8
[24] Svaasand L O, Eriksrud M, Grande A P and Mo F 1973 *J. Cryst. Growth* **18** 179–84